# On the photo and back isomerization of phenylazothiazoles anchored onto peptoids : one step further toward visible-light photoswitches for solar energy harnessing

Gwendal Henrard[a,b], Thomas Robert[a], Benjamin Tassignon[a,b], Julien De Winter[a], Jérôme Cornil[b], Pascal Gerbaux[a]

[a] Organic Synthesis and Mass Spectrometry Laboratory ($S^2MOs$) Chemistry Department, Materials Research Institute, University of Mons – UMONS, Place du Parc 23, 7000 Mons (Belgium)

[b] Laboratory for Chemistry of Novel Materials Chemistry Department, Materials Research Institute, University of Mons – UMONS, Place du Parc 23, 7000 Mons (Belgium)

## Supporting information

***Content :***

### *1. Synthesis*

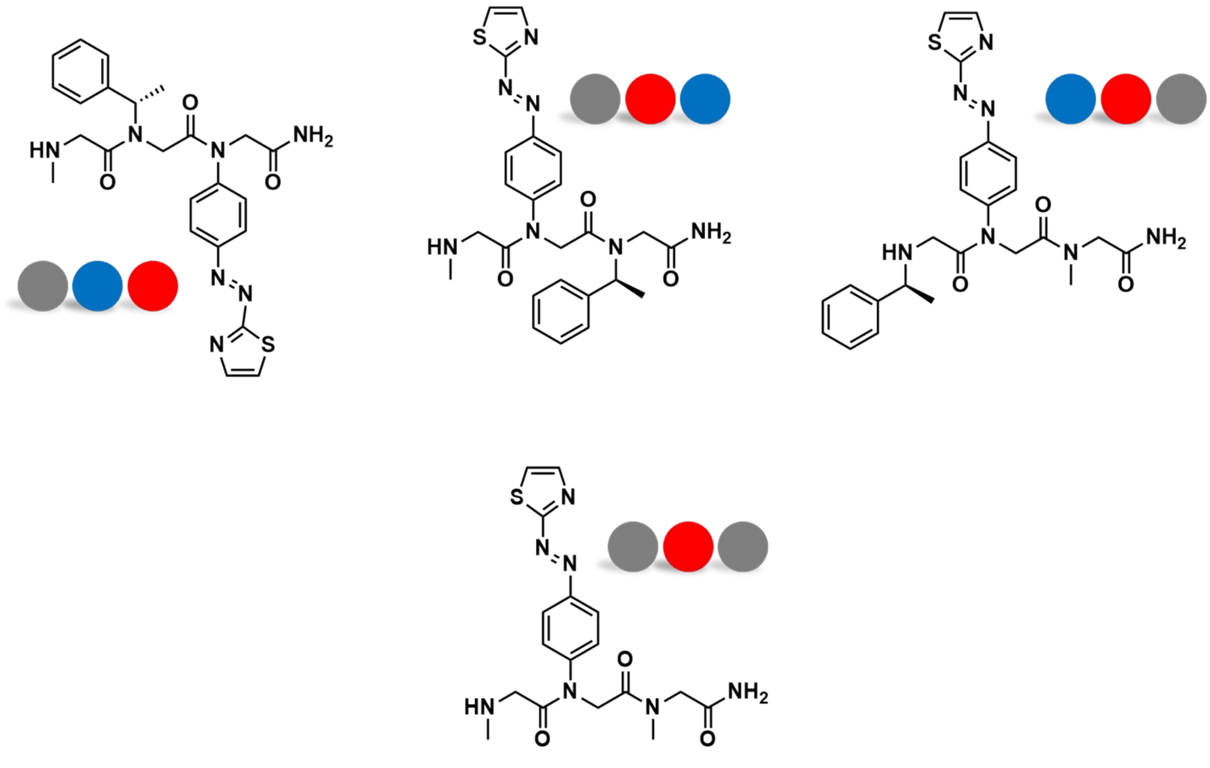

***Figure SI1.*** *Molecular structures of the Nsar/Nspe/N2tz hybrid peptoids. A ball formalism is used to allow a better visualization of the peptoid sequence, with grey balls indicating Nsar residue, blue balls corresponding to spe side chains and red balls indicating the PAT unit.*

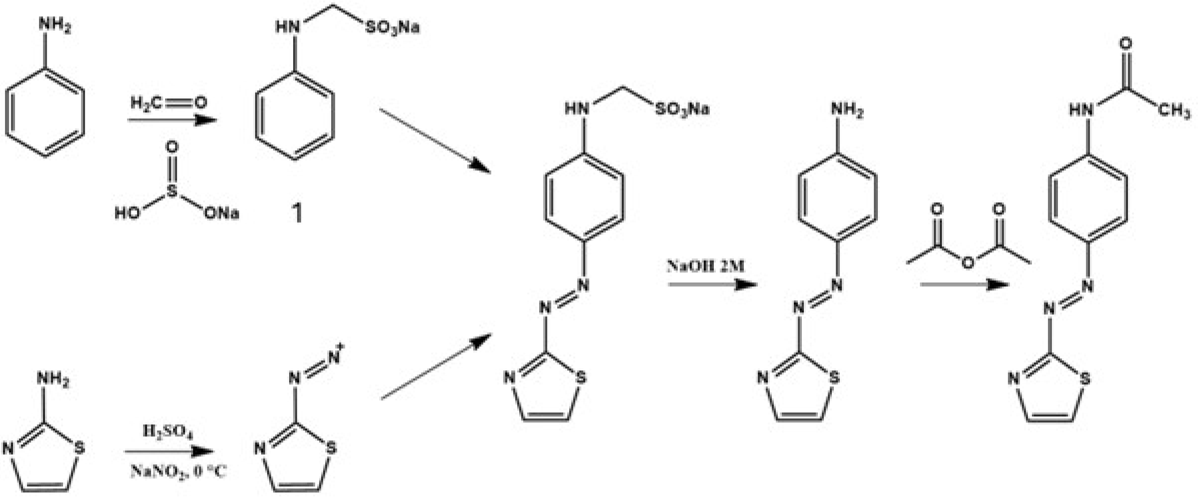

***Figure SI2.*** *Synthesis pathway of $NH_2$-PAT and Ac-PAT.*

## ***2. Structural characterization : methods and data***

### *NUCLEAR MAGNETIC RESONANCE SPECTROSCOPY*

$^1$H NMR spectra are recorded at R.T (23 °C) on a Bruker AVANCE II 500 spectrometer operating at 500 MHz in the General, Organic and biomedical Chemistry Laboratory (UMONS). Chemical shifts are reported in parts per million (ppm) relative to tetramethylsilane (TMS) as an internal standard. Samples are prepared at a concentration of 10 mg.ml$^{-1}$ in the appropriate deuterated solvent.

*MASS SPECTROMETRY*

To structurally characterize **sodium anilinomethanesulfonate**, **$NH_2$-PAT** and **Ac-PAT**, Electrospray Ionization (ESI) mass spectrometry operating in positive or negative ionization mode was used on a Waters Synapt G2-Si mass spectrometer (Waters, UK). The sample were solubilized in a Water/MeOH 1:1 solution at a concentration of 1 mg.ml$^{-1}$, further 100x diluted with the same mixture of solvents before direct infusion (5 µl.min$^{-1}$) into the ESI source. Typical source parameters were capillary voltage (3.1 kV), cone voltage (30 V), source temperature (80 °C), desolvation temperature (120 °C), $N_2$ flow rate (Cone 50 l.h$^{-1}$, desolvation 500 l.h$^{-1}$) and resolution (FWHM = 20 000 @ m/z 922). HRMS analyses (exact mass measurements) were performed to determine the elemental composition of the detected ions. NaI cluster ions were used as external calibrants (lock mass) in both ionization modes.

ElectroSpray Ionization Mass Spectrometry (ESI-MS) was employed to characterize the primary structure of the synthesized peptoids. Sample solutions were prepared in HPLC-grade MeOH at a concentration of 1 mg.mL$^{-1}$. After dilution (1000 x), the solutions were injected into the ESI source using a syringe pump at a flow rate of 5 µL.min$^{-1}$. To confirm the primary structure of the synthesized peptoids, tandem mass spectrometry (MS/MS) experiments were carried out by selecting the mass-to-charge ratio of precursor ions and subjecting them to collisional activation to induce fragmentation. Collision-induced dissociation (CID) experiments correspond to the fragmentation resulting from an energy transfer to the ions upon inelastic collisions with an inert gas (argon). The collision energy was adjusted to ensure sufficient fragmentation while maintaining detection of the precursor ions. The CID mass spectra were assigned based on the literature [1-2].

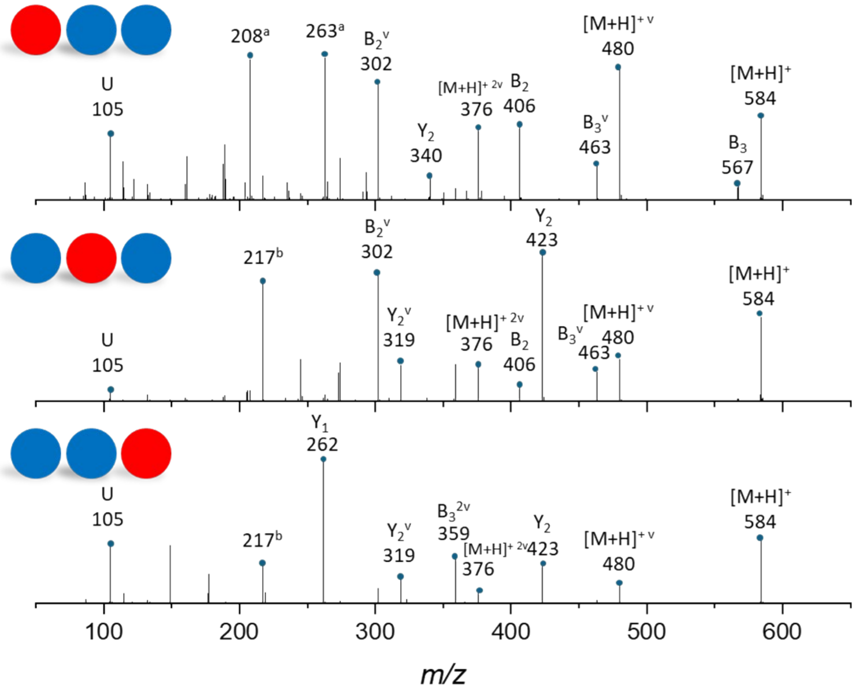

***Figure SI3.*** *ESI-MS/MS (Waters Synapt G2-Si) CID spectra of m/z 584 ([M+H]$^+$) ions corresponding to protonated N2tzNspeNspe (top), NspeN2tzNspe (middle) and NspeNspeN2tz (bottom). Spectra were recorded with collision energy ($E_{col}$) of 17 eV.* [a] *Fragmentation of the thiazole group, likely due to generation of a relatively stable thiazolyl-carbene species.* [b] *Fragment corresponding to successive B/Y and A/Y fragmentation. A ball formalism is used to allow a better visualization of the peptoid sequence, with blue balls corresponding to spe side chains and red balls indicating the PAT unit.*

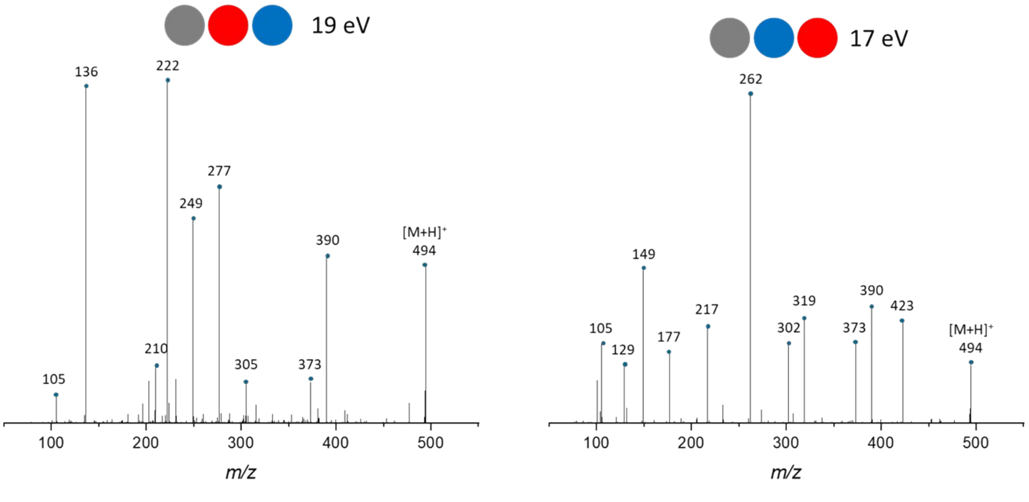

***Figure SI4.*** *ESI-MS/MS (Waters Synapt G2-Si) CID spectra of m/z 494 ([M+H]$^+$) ions corresponding to protonated NsarN2tzNspe and NsarNspeN2tz. Spectra were recorded with collision energy ($E_{col}$) specified with the data. A ball formalism is used to allow a better visualization of the peptoid sequence, with grey balls standing for the sar side chains, blue balls corresponding to spe side chains and red balls indicating the PAT unit.*

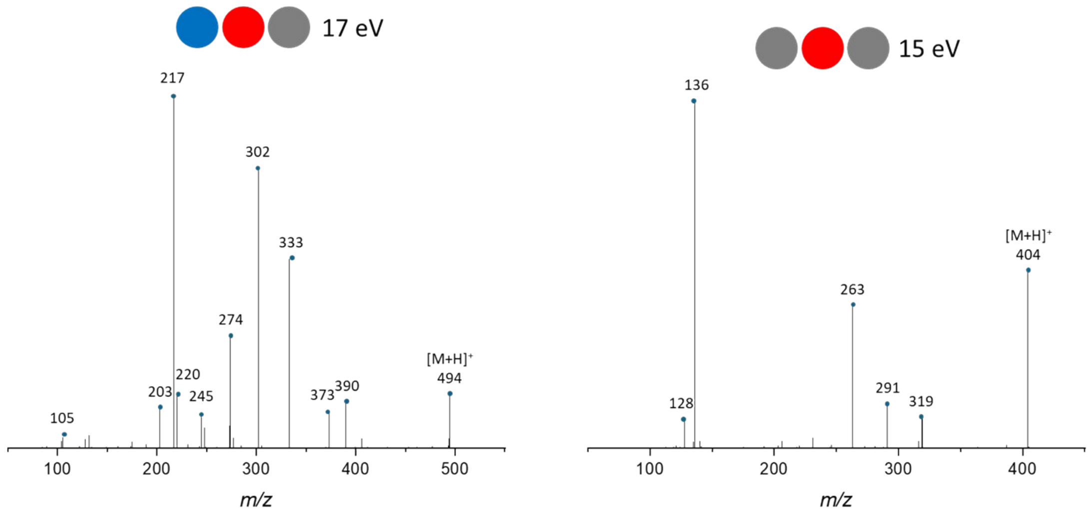

***Figure SI5.*** *ESI-MS/MS (Waters Synapt G2-Si) CID spectra of m/z 494 and m/z 404 ($[M+H]^+$) ions corresponding to protonated NspeN2tzNsar and NsarN2tzNsar, respectively. Spectra were recorded with collision energy ($E_{col}$) specified with the data. A ball formalism is used to allow a better visualization of the peptoid sequence, with grey balls standing for the sar side chains, blue balls corresponding to spe side chains and red balls indicating the PAT unit.*

### INFRARED SPECTROSCOPY

Infrared spectra were recorded using a compact Fourier Transform Infrared (FT-IR) spectrometer (Bruker model ALPHA – ATR mode). Samples were analyzed in the solid state without further preparation. Spectra were collected in the range of 4000 to 600 cm$^{-1}$, with a spectral resolution of 2 cm$^{-1}$ and averaging 32 scans for each measurement. The recorded absorption bands were assigned to the main functional groups of the analytes in order to confirm their chemical structure.

### MELTING POINT

The melting points were determined using a capillary tube and an MPA100 Melting Point Apparatus. A small amount of the sample in fine powder was packed into a capillary with a height of 2-3 mm and the capillary was inserted into the preheated block. An initial quick scan (10 °C.min$^{-1}$) was performed to estimate the approximate melting temperature range. The final measurement was then carried out at a controlled heating rate of 2 °C.min$^{-1}$. The melting point was recorded as the temperature at which the sample becomes completely clear and liquid.

## *3. Irradiation experiments*

Irradiation experiments to study the E → Z photoisomerization via UV-Vis spectroscopy were carried out using a LightningCure LC8 L9588-03 lamp (Hamamatsu Photonics, K.K.) for visible irradiation and a LightningCure LC8 9588-02A lamp (Hamamatsu Photonics, K.K.) for UV irradiation [3-4].

- LightningCure LC8 9588-03 (visible lamp) is a Hg-Xe lamp (Figure SI6) used at 20 % power, corresponding to a relative irradiance of 900 mW.cm$^{-2}$. The irradiance is measured at the distance of 1 cm from the output end of the optical fiber (5 mm output diameter).

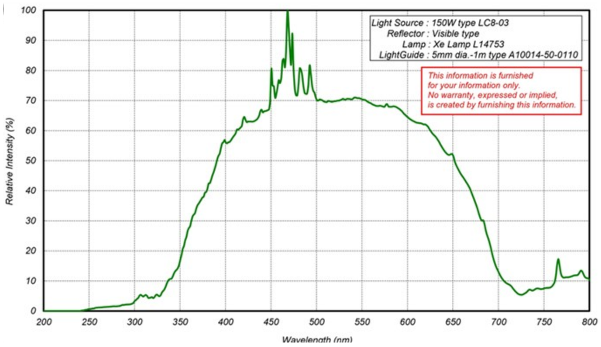

***Figure SI6.*** *Emission spectrum of the Hamamatsu LightningCure LC8 9588-03 [3].*

- LightningCure LC8 9588-02A (*UV lamp*) is a Hg-Xe lamp (Figure SI7a) used at 20 % power, corresponding to a relative irradiance of 900 mW.cm$^{-2}$. The irradiance measured at the distance of 1 cm from the output end of the optical fiber (5 mm output diameter). The dispositive is further equipped with a UV transmitting filter (50x50 mm, center wavelength = 325 nm, OptoSigma), its transmission spectrum is shown on Figure SI7b.

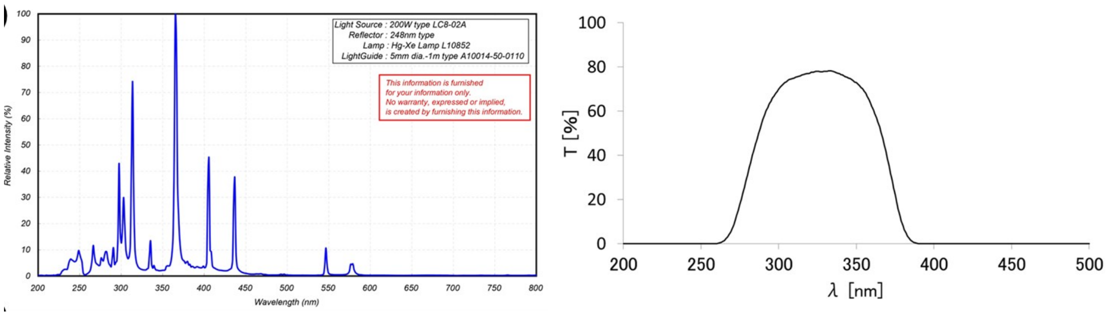

***Figure SI7.*** *a) Emission spectra of the UV lamp (LightningCure LC8 9588-02A) [4a]. b) Transmission spectrum of the UV transmitting filter [4b].*

## *4. Solvent polarity scale*

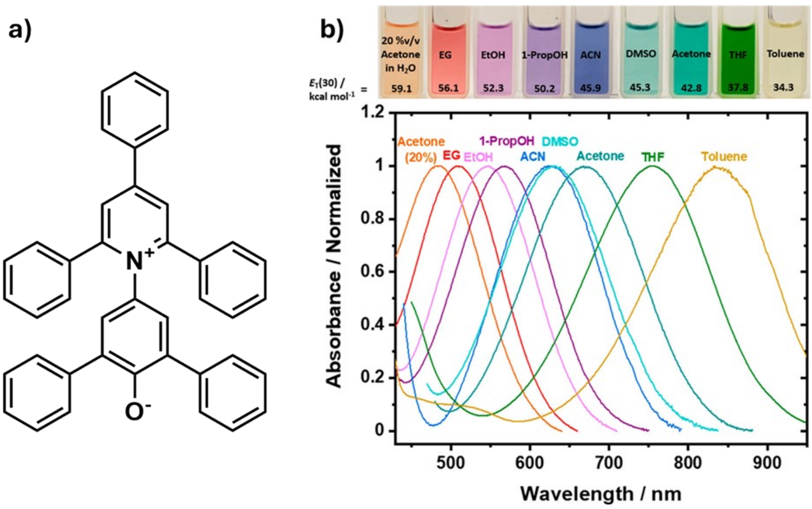

***Figure SI8.*** *a) Molecular structure of the B30 in its zwitterionic form adapted from [4]. b) Normalized absorption band of the B30 dissolved in nine different solvents. From left to right: 20 % acetone/*$H_2O$*, ethylene glycol (EG), EtOH, 1-propanol (1-PrOH), ACN, dimethyl sulfoxide (DMSO), THF and toluene. The corresponding* $E_T(30)$ *values are indicated, showing a progressive redshift of the absorption band with decreasing solvent polarity. Numeric values of* $E_T(30)$ *and* $E_T^N(30)$ *measured at 293 K are reported in Table SI1.*

The thermal back-isomerization is strongly influenced by the nature of the solvent. Solvent polarity, proticity and even viscosity affect the activation barrier of the thermal back-isomerization and, consequently, the $t_{1/2}$ of the Z-isomer. Since this process is concomitantly impacted by several parameters, it is really difficult to define a single descriptor that accounts for all solvent effects at once. In this context, the use of empirical polarity parameters such as the Dimroth and Reichardt parameter ($E_T(30)$) offers a representative approach to describe the overall solvent effect [5].

$E_T(30)$ is based on absorption of betaine 30 (B30) (Figure SI8), a solvatochromic dye whose maximum absorption is highly sensitive to the solvent environment, as illustrated in Figure SI8. $E_T(30)$ (kcal.mol$^{-1}$) value of a solvent can be calculated according to Eq.4 :

$$E_T(30) = 0.239 * N_a hc\nu_{max} = 2.8591 * 10^{-3} * \nu_{max} = \frac{28591}{\lambda_{max}} \qquad (Eq.4)$$

In Eq.1, h denotes Planck's constant, c is the speed of light in vacuum, and $N_a$ is Avogadro number. The factor 0.239 accounts for the conversion from joules to kilocalories. The term $\upsilon_{max}$ (cm$^{-1}$) or its reciprocal $\lambda_{max}$ (nm) corresponds to the wavenumber or wavelength, respectively, of the maximum absorption band of B30.

To allow comparison across different solvents, the $E_T(30)$ values are often normalized according to Eq.5, where TMS ($E_T(30)$= 30.7) and $H_2O$ ($E_T(30)$ = 63.1) are taken as reference solvents corresponding to lowest and highest polarity values, respectively (TMS = tetramethylsilane). This normalization yields a dimensionless parameter, $E_T^N(30)$, ranging from 0 for the least polar solvents to 1 for the most polar solvents, which allows a more straightforward comparison of solvent effects on the thermal back isomerization rate.

$$E_T^N(30) = \frac{E_T(solvent) - E_T(TMS)}{E_T(H_2O) - E_T(TMS)} = \frac{E_T(solvent) - 30.7}{32.4} \#(Eq.5)$$

In this study, different solvents have been selected and their corresponding $E_T(30)$ and $E_T^N(30)$ values are reported in Table SI1, based on reference data available in literature [5].

| Solvent | λmax (nm) | $E_T(30)\ (kcal.mol^{-1})$ | $E_T^N(30)$ |
|---|---|---|---|
| TMS | 931 | 30.7 | 0.00 |
| Toluene | 843 | 33.9 | 0.10 |
| Ethyl acetate (EtAc) | 750 | 38.1 | 0.23 |
| Chloroform ($CHCl_3$) | 731 | 39.1 | 0.26 |
| DCM | 702 | 40.7 | 0.31 |
| Acetone | 677 | 42.2 | 0.35 |
| ACN | 627 | 45.6 | 0.46 |
| Isobutanol (Isobut) | 654 | 43.7 | 0.40 |
| 1-propanol (1-PrOH) | 564 | 50.7 | 0.62 |
| 2-propanol (2-PrOH) | 581 | 49.2 | 0.57 |
| EtOH | 550 | 51.9 | 0.65 |
| MeOH | 516 | 55.4 | 0.76 |
| $H_2O$ | 453 | 63.1 | 1.00 |

***Table SI1.*** *$\lambda_{max}$ values of B30 in the thirteen solvents measured at 293 K. Numeric values of $E_T(30)$ and $E_T^N(30)$ taken from literature [5].*

However, for mixture of solvents, reference values are generally not available in the literature and must therefore be experimentally determined and gathered in Table SI2. To establish these values, betaine 30 is first dissolved in the solvent mixture at a concentration of 1 mg.ml$^{-1}$ and then diluted to approximately 5 10$^{-5}$ mol.l$^{-1}$. The $\lambda_{max}$ values are then introduced into Eq.1 and Eq.2 to calculate the corresponding parameters. In this study, the solvent mixtures investigated include MeOH/$H_2O$ (1:3, 1:1 and 3:1), MeOH/ACN (1:1) and ACN/$H_2O$ (1:1). For validation of the method, the $E_T(30)$ of the pure solvents were also experimentally determined under identical conditions and compared to the literature data in Table SI2.

| Solvents | $\lambda_{max}$ (nm) | $E_T(30)$ (kcal.mol$^{-1}$) | $E_T^N$ (30) |
|---|---|---|---|
| $H_2O$ | 452 | 63.3 | 1.004 |
| MeOH | 510 | 56.1 | 0.783 |
| ACN | 624 | 45.8 | 0.467 |
| MeOH/$H_2O$ (1:3) | 469 | 61.0 | 0.934 |
| MeOH/$H_2O$ (1:1) | 485 | 59.0 | 0.872 |
| MeOH/$H_2O$ (3:1) | 504.5 | 56.7 | 0.802 |
| MeOH/ACN (1:1) | 516 | 55.4 | 0.763 |
| ACN/$H_2O$ (1:1) | 501 | 57.1 | 0.814 |

***Table SI2.*** *Dimroth-Reichardt method to assess solvent polarity: $\lambda_{max}$ values of B30 in the 8 solvents measured at R.T with numeric values of $E_T(30)$ and $E_T^N(30)$.*

## *5. Real-life irradiation experiments*

We conducted solar irradiation experiments under real-life conditions on **Cter-PAT** as a representative compound. A methanolic solution of **Cter-PAT** was exposed to sunlight between 12:00 to 13:00 CET under various weather conditions (Figure SI9a). The first experiment was performed on October 16, 2024, during a partly sunny and cloudy day (T = 21 °C and UV index = 2/10). The second experiment took place on October 21, 2024, under rainy conditions (T = 13 °C, UV index = 1/10). The final experiment was carried out on September 16, 2025, during a fully sunny day (T = 29 °C and UV index of 5/10). In all cases, the samples were irradiated on the rooftop of the UMONS chemistry building (50°27'53.5"N ; 3°57'25.6"E), and LC-MS analyses were immediately performed following irradiation. During the last experiment, a time-resolved follow-up of the photoisomerization process revealed that the PSS is reached within 30 s of solar irradiation (Figure SI9b). This rapid photoisomerization is particularly promising for MOST energy storage, as it demonstrates the system ability to efficiently harvest and store solar energy in a short timescale. Overall, solar irradiation proved to be highly effective in triggering the photoisomerization process, with a Z-isomer content of 66 % at the PSS under all the tested conditions.

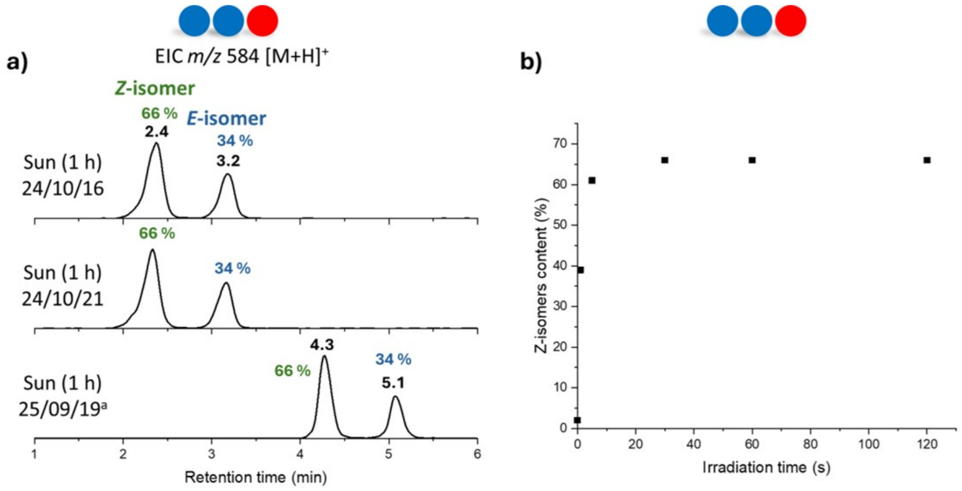

*Figure SI9. a) LC-MS analysis (EIC chromatograms of the [M+H]$^+$ ions at m/z 584) of* ***Cter-PAT*** *in MeOH under different sunlight irradiation conditions: cloudy October 16, 2024, partly sunny and cloudy day (upper), October 21, 2024, rainy conditions and September 16, 2025, fully sunny day. b) Z-isomer content in function of the irradiation time under sunlight for the Cter-PAT 1 in MeOH. The PSS is reached within 30 s of solar irradiation.*

### *6. Thermal back-isomerization : protocols and mathematical analysis*

After irradiation of the peptoid solutions and determination of PSS, the vial containing the sample is placed in the HPLC autosampler, where it is stored in the dark under controlled temperature conditions. LC-MS measurements are repeated at regular intervals on the stored solutions to monitor the kinetics of the Z → E thermal back isomerization. The relative Z-isomer content is normalized and plotted as a function of storage time. The resulting decay curves obtained are fitted in OriginPro 2019 using a single-exponential decay function, consistent with the well-established first-order kinetics of the thermal back-isomerization of **ABs**. The fitting equation applied is Eq.1.

$$y\,(t) = y_0 + A\,e^{-kt}\#(Eq.1)$$

where y (t) is the normalized Z-isomer fraction at time t, $y_0$ is the offset value for the Z-isomer content (fixed at 0 in this case), A is the initial Z-isomer content (set at 1) and k ($s^{-1}$) corresponds to the first order rate constant. From the fitted values of k, the $t_{1/2}$ of the Z-isomer is determined according to Eq.2:

$$t_{\frac{1}{2}} = \frac{\ln(2)}{k}\#(Eq.2)$$

To determine the activation energy of the thermal back-isomerization process, the kinetics are monitored by LC-MS measurements at different temperatures by adjusting the temperature of the HPLC autosampler (10, 15, 20, 25 and 30 °C). Eyring-Polanyi equation (Eq.3) is used. This approach enables extraction of activation enthalpy ($\Delta H^{\ddagger}$) and activation entropy ($\Delta S^{\ddagger}$), thus providing complementary information about the mechanism of the thermal back-isomerization process.

$$\ln\frac{k}{T} = \left(\ln\frac{k_b}{h} + \frac{\Delta S^{\ddagger}}{R}\right) - \left(\frac{\Delta H^{\ddagger}}{R}\right)\frac{1}{T}\#(Eq.3)$$

where k ($s^{-1}$) is the rate constant, T is the temperature (K), $k_B$ is the Boltzmann constant ($1.38*10^{-23}$ $J.K^{-1}$), h is the Planck constant ($6.62*10^{-34}$ J.s), $\Delta S^{\ddagger}$ is the activation entropy ($J.mol^{-1}.K^{-1}$), R is the molar gas constant (8.314 $J.mol^{-1}.K^{-1}$) and $\Delta H^{\ddagger}$ is the activation enthalpy ($kJ.mol^{-1}$).

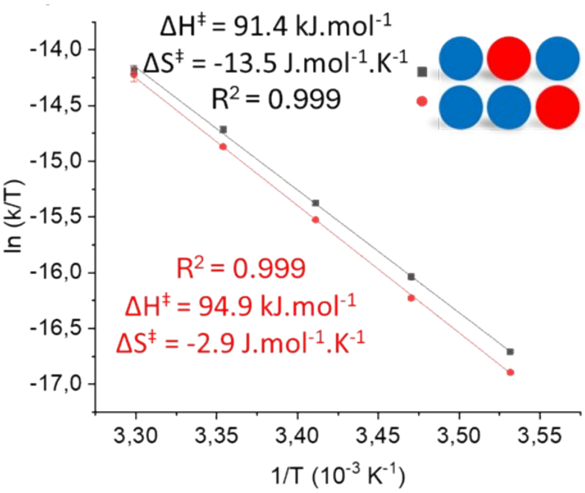

***Figure SI10.*** *Eyring-Polanyi plot based on the rate constants extracted from the kinetics at different temperatures for* ***Cter-PAT*** *and* ***Center-PAT*** *(LC-MS procedure). Kinetics parameters are presented for* ***Cter-PAT*** *in red and* ***Center-PAT*** *in black. A ball formalism is used to allow a better visualization of the peptoid sequence, with blue balls corresponding to spe side chains and red balls indicating the PAT unit.*

## *7. Thermal back-isomerization of Nspe/Nsar/N2tz hybrid peptoids*

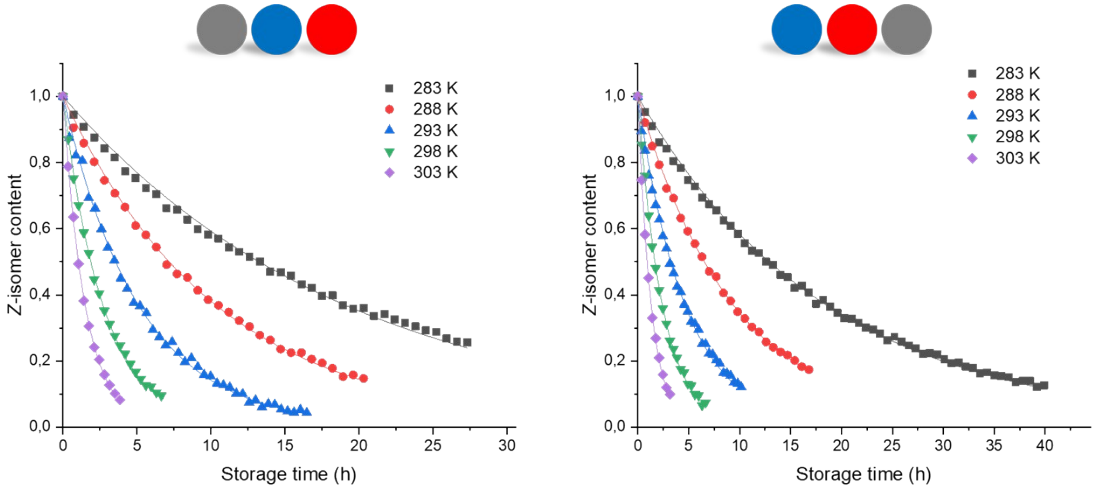

***Figure SI11.*** *Monitoring of the thermal Z → E back-isomerization kinetics by LC-MS analyses at various temperatures ranging from 283 K to 303 K in 5-degree increments for hybrid peptoids in MeOH. A ball formalism is used to allow a better visualization of the peptoid sequence, with grey balls standing for the sar side chains, blue balls corresponding to spe side chains and red balls indicating the PAT unit.*

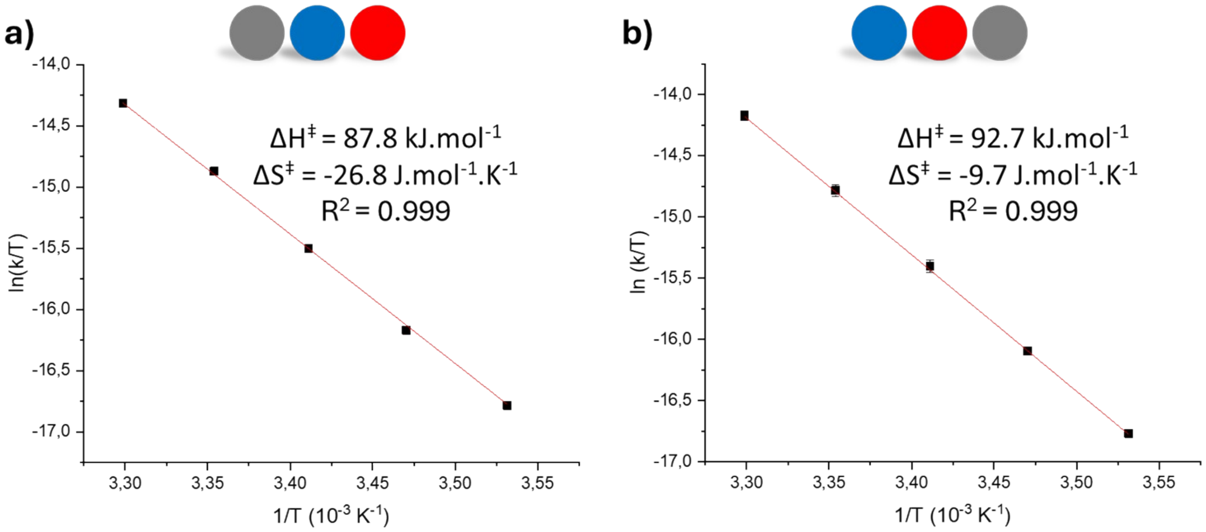

***Figure SI12.*** *Eyring-Polanyi plot based on the rate constants extracted from the kinetics at different temperatures for NsarNspeN2tz (a) and NspeN2tzNsar (b), with presentation of the kinetic parameters. A ball formalism is used to allow a better visualization of the peptoid sequence, with grey balls standing for the sar side chains, blue balls corresponding to spe side chains and red balls indicating the PAT unit.*

## *8. Solvent effects on back isomerization*

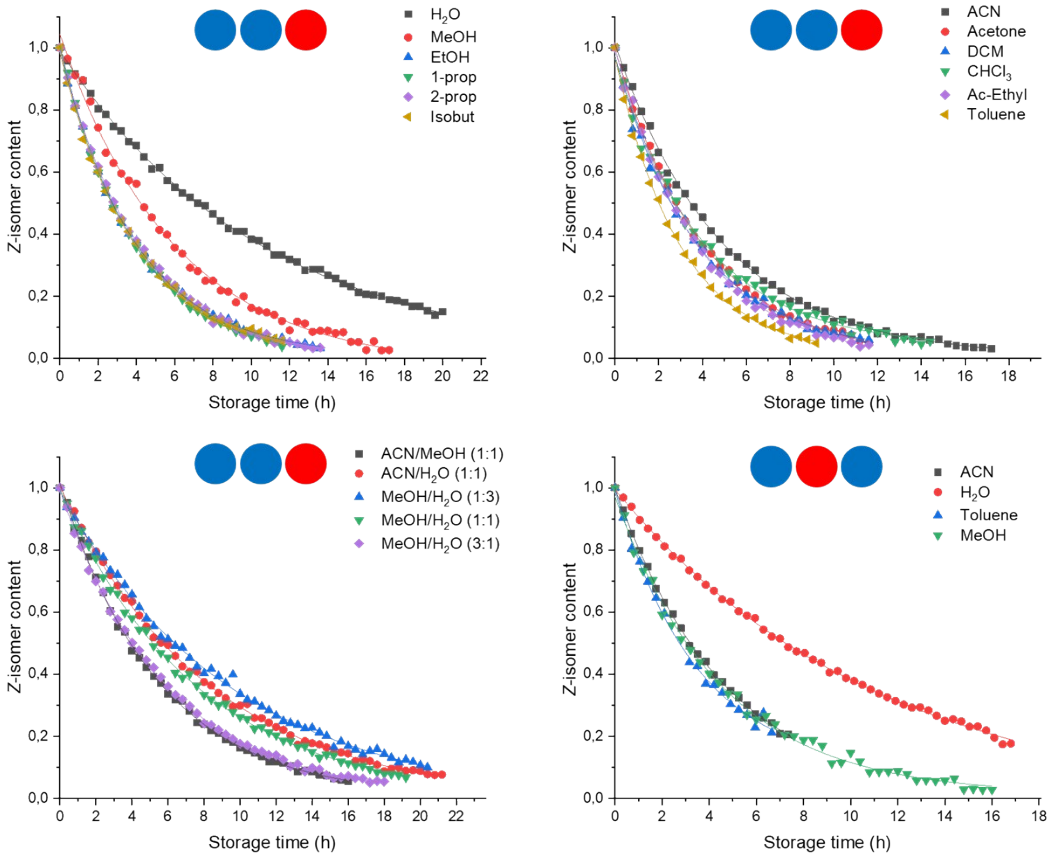

***Figure SI13.*** *Monitoring of the thermal Z → E back-isomerization kinetics by LC-MS analyses at 20 °C for* ***Cter-PAT*** *and* ***Center-PAT*** *in various solvents. Normalized Z-isomer content plotted against the time showing a first-order exponential decay. A ball formalism is used to allow a better visualization of the peptoid sequence, with blue balls corresponding to spe side chains and red balls indicating the PAT unit.*

| 20°C | k ($10^{-5}$ $s^{-1}$) | $t_{1/2}$ (h) | $E_T^N(30)$ |
|---|---|---|---|
|  | 🔵🔵🔴 |  |  |
| $H_2O$ | 2.73 ± 0.05 | 7.05 ± 0.13 | 1.00 |
| MeOH | 5.30 ± 0.03 | 3.63 ± 0.03 | 0.76 |
| EtOH | 6.93 ± 0.04 | 2.78 ± 0.02 | 0.65 |
| 1-prop | 7.16 ± 0.03 | 2.69 ± 0.01 | 0.62 |
| 2-prop | 6.83 ± 0.03 | 2.81 ± 0.01 | 0.57 |
| Isobut | 7..07 ± 0.05 | 2.72 ± 0.02 | 0.40 |
| ACN | 5.25 ± 0.34 | 3.68 ± 0.24 | 0.46 |
| Acetone | 6.94 ± 0.04 | 2.77 ± 0.02 | 0.35 |
| DCM | 7.33 ± 0.10 | 2.63 ± 0.03 | 0.31 |
| $CHCl_3$ | 7.14 ± 0.25 | 2.74 ± 0.10 | 0.26 |
| Ac-ethyl | 7.50 ± 0.05 | 2.57 ± 0.02 | 0.23 |
| Toluene | 8.78 ± 0.59 | 2.20 ± 0.15 | 0.10 |
| ACN/$H_2O$ (1:1) | 3.40 ± 0.02 | 5.66 ± 0.03 | 0.81 |
| ACN/MeOH (1:1) | 4.95 ± 0.02 | 3.89 ± 0.02 | 0.76 |
| MeOH/$H_2O$ (1:3) | 2.99 ± 0.06 | 6.45 ± 0.12 | 0.93 |
| MeOH/$H_2O$ (1:1) | 3.76 ± 0.01 | 5.12 ± 0.01 | 0.87 |
| MeOH/$H_2O$ (3:1) | 4.64 ± 0.11 | 4.15 ± 0.10 | 0.80 |
|  | 🔵🔴🔵 |  |  |
| $H_2O$ | 2.66 ± 0.02 | 7.25 ± 0.05 | 1.00 |
| MeOH | 6.14 ± 0.10 | 3.13 ± 0.08 | 0.76 |
| ACN | 6.08 ± 0.10 | 3.17 ± 0.05 | 0.46 |
| Toluene | 6.63 ± 0.13 | 2.90 ± 0.06 | 0.10 |

***Table SI3.*** *Kinetic constants and* $t_{1/2}$ *values obtained for* ***Cter-PAT*** *and* ***Center-PAT*** *at 20 °C in various solvents, along with their corresponding* $E_T^N(30)$*.*

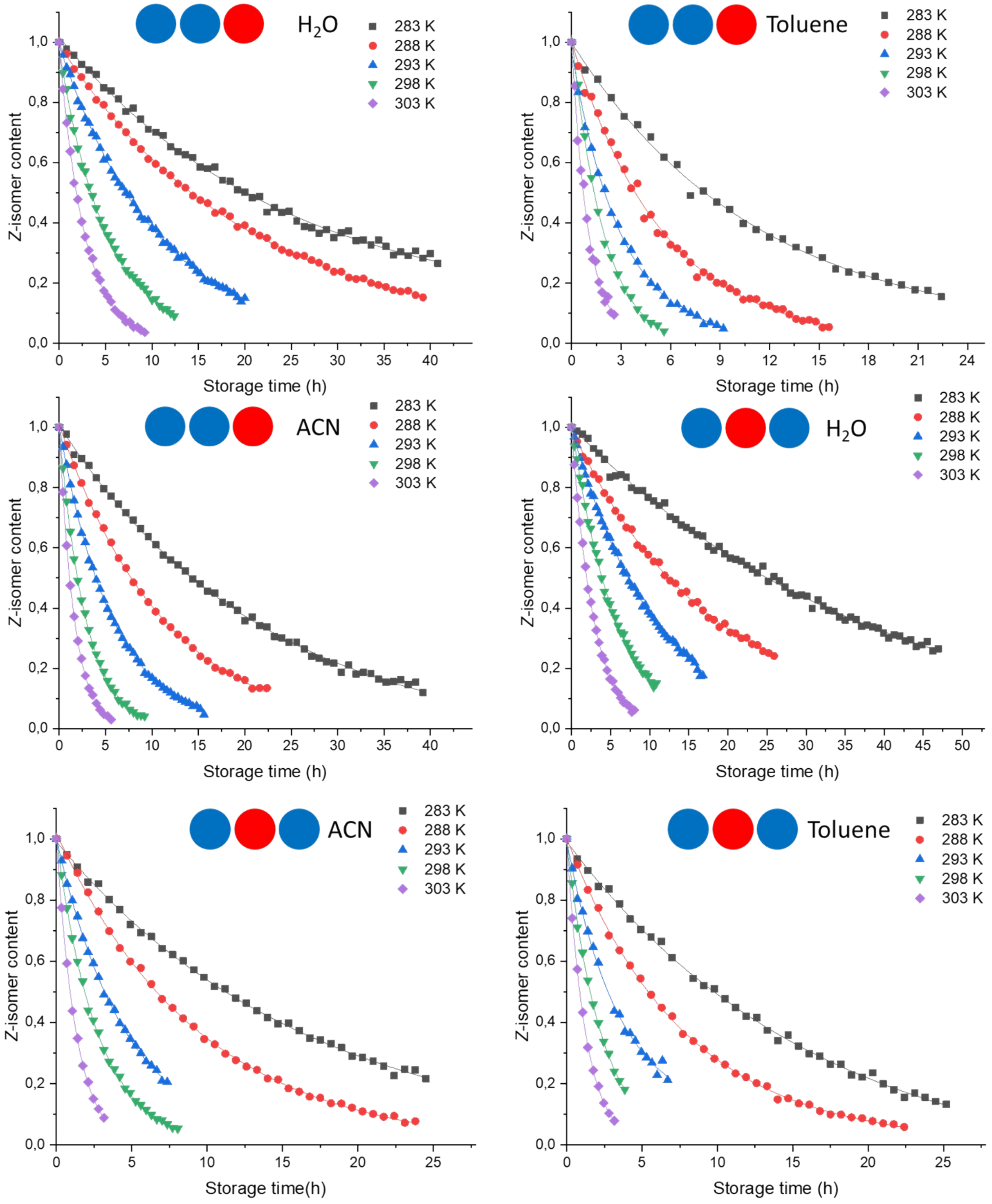

*Figure SI14. Monitoring of the thermal Z → E back-isomerization kinetics by LC-MS analyses at various temperatures ranging from 283 K to 303 K in 5-degree increments for **Cter-PAT** and **Center-PAT** in $H_2O$, ACN and toluene. A ball formalism is used to allow a better visualization of the peptoid sequence, with blue balls corresponding to spe side chains and red balls indicating the PAT unit.*

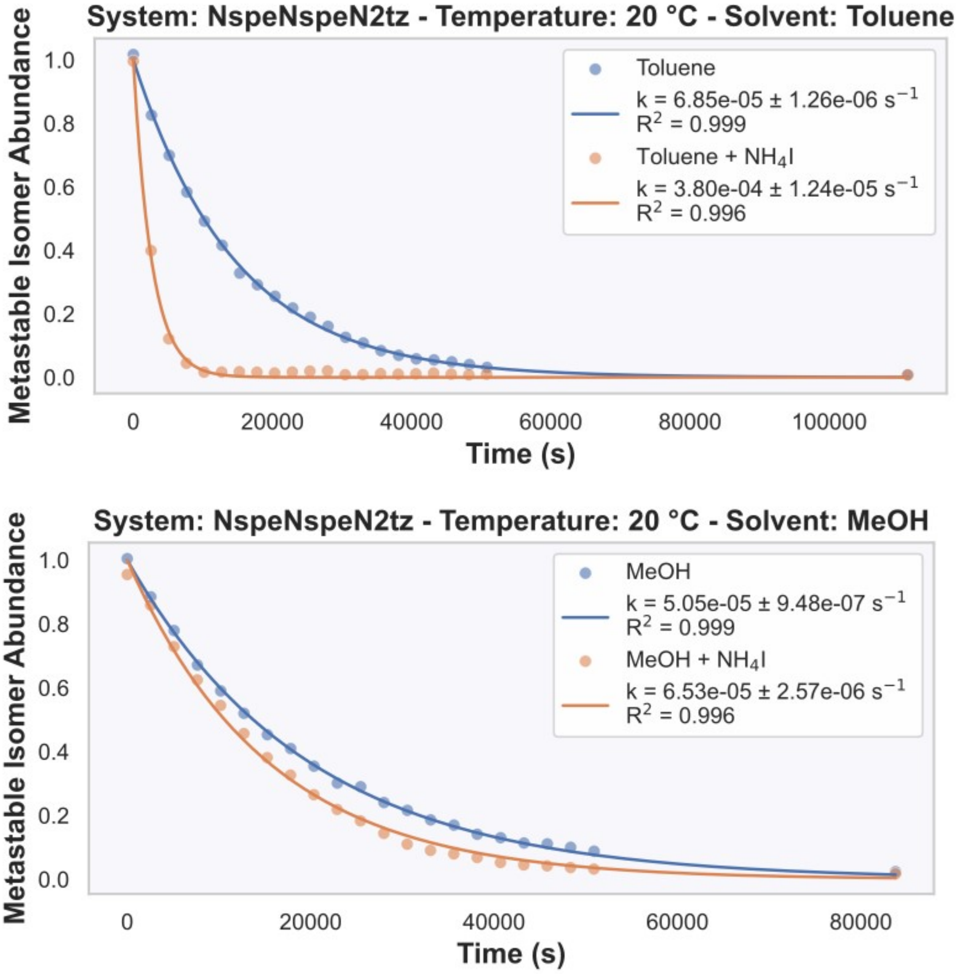

***Figure SI15.*** *Monitoring of the thermal Z → E back-isomerization kinetics by LC-MS analyses for* ***Cter-PAT*** *in toluene and methanol in presence and absence of ammonium iodide (100 equivalents).*

## *9. References*

1. Halin, E.; Hoyas, S.; Lemaur, V.; Winter, J. De; Laurent, S.; Connolly, M. D.; Zuckermann, R. N.; Cornil, J.; Gerbaux, P. Backbone Cleavages of Protonated Peptoids upon Collision-Induced Dissociation: Competitive and Consecutive B-Y and A1-Yx Reactions. *J.Am.Soc.Mass Spectrom.* **2019**, *30*, 2726–2740.
2. Halin, E.; Hoyas, S.; Lemaur, V.; Winter, J. De; Laurent, S.; Connolly, M. D.; Zuckermann, R. N.; Cornil, J.; Gerbaux, P. Backbone Cleavages of Protonated Peptoids upon Collision-Induced Dissociation: Competitive and Consecutive B-Y and $A_1$-$Y_x$ Reactions. J.Am.Soc.Mass Spectrom. **2019**, *30*, 2726–2740.
3. Hamamatsu LC8 9588-03 https://www.hamamatsu.com/eu/en/product/light-and-radiation-sources/lamp-module_unit/spot-light-source/L9588.html.

4. (a) Hamamatsu LC8 9588-02A https://www.hamamatsu.com/eu /en/product/light-and-radiation-sources/lamp-module_unit/spot-light source/L9588.html ; (b) OptoSigma UV transmitting filter https://www.optosigma.com/eu_en/optics/filters/colored-glass-filters/uv-transmitting-filter-50mm-wavelength-350nm.html.

5. Pandian, R.; Burda, H.; Alfurayj, I.; Reichardt, C.; Burda, C. 60 Years of Betaine 30 – From Solvatochromic Discovery to Future Frontiers. *J.Phys.Chem.B* **2024**, *128*, 6990–7001.